Available online at www.sciencedirect.com
SCIENCE DIRECT®
Catalysis Today 93–95 (2004) 395–403
CATALYSIS TODAY
www.elsevier.com/locate/cattod

# Stereoselective hydrogenation of Paracetamol to *trans*-4-acetamidocyclohexanol on carbon-supported Ru–M (M = Co, Ni) bimetallic catalysts

M. Cerro-Alarcón [a,b], A. Guerrero-Ruíz [a], I. Rodríguez-Ramos [b,*]

[a] *Departamento de Química Inorgánica y Química Técnica, Facultad de Ciencias, UNED, c/Senda del Rey, No. 9, 28040 Madrid, Spain*
[b] *Instituto de Catálisis y Petroleoquímica, CSIC, c/Marie Curie, Campus de Cantoblanco, 28049 Madrid, Spain*

Available online 19 July 2004

**Abstract**

This paper describes the results obtained on the catalytic hydrogenation of Paracetamol (4-acetamidophenol), carried out at 393 K, over carbon-supported Ru, Co and Ni based monometallic catalysts, and over graphite-supported Ru–M (M = Co, Ni) bimetallic catalysts. A comparative study of the effect of the different supported-metal catalysts and of the applied reduction temperature has been carried out. Two selectivity parameters have been controlled: the production of by-products and the *trans–cis* composition of 4-acetamidocyclohexanol (stereoselectivity). Characterisation of the catalysts was performed by temperature-programmed reduction (TPR) and CO volumetric chemisorption. It was found that the hydrogenation reaction of Paracetamol is structure sensitive, since intrinsic activity and selectivity values are modified with variations in the metallic particle sizes. Generally, the catalytic activity, under our experimental conditions, follow the trend: Pt < Pd < Ni ≪ Co < Ru. The production of secondary compounds derived of hydrogenolytic cleavage (*N*-cyclohexylacetamide) and/or of partial hydrogenation reactions (4-acetamidocyclohexanone), depends on the active metal: Ni < Ru < Co, among other factors. Concerning the stereoselectivity (*trans* to *cis* ratio), among the monometallic catalysts Co exhibited the highest T/C ratio, with the overall sequence: Co > Ni > Ru. Finally, the bimetallic catalysts, particularly those of Ru–Ni, show an improved stereoselectivity (T/C ratio) in comparison with the corresponding counterparts.


*Keywords:* Stereoselective hydrogenation; *trans* and *cis* isomers; 4-Aminocyclohexanol; Ambroxol; Carbon-supported catalysts; Bimetallic catalysts

## 1. Introduction

Ambroxol, *N*-(2-amino-3,5-dibromobenzyl)-*trans*-4-aminocyclohexanol, is a very significant and widespread bronchosecretolitic agent for the prevention and treatment of some diseases of the respiratory track and bronchial tubes [1,2] such as asthma and acute and chronic bronchitis. Moreover, recent investigations have confirmed the local anaesthetic properties of this compound for sore throat treatment [1]. And there are some recent findings that suggest that Ambroxol may prevent *Helicobacter pylori*-associated gastric carcinogenesis [3]. There are several routes according to which the Ambroxol molecule may be prepared from the intermediate *trans*-4-aminocyclohexanol [4–8]. In some cases, the *trans*-4-aminocyclohexanol molecule is directly reacted to yield Ambroxol [5], or else is used as an intermediate for the synthesis of other intermediates [4,6,9,10].

Synthesis of *trans*-4-aminocyclohexanol is usually approached by catalytic hydrogenation of 4-acetamidophenol (Paracetamol) [9,11–15], as shown in Fig. 1. According to the procedures, the catalytic hydrogenation of Paracetamol yields a *cis*/*trans* mixture of 4-acetamidocyclohexanol. Hydrolysis of this mixture yields *cis*/*trans*-4-aminocyclohexanol. Isomers are finally separated by fractional crystallisation.

It is common knowledge that the synthesis of a *trans* stereoisomer is achieved along with the *cis* form. But purity has a great significance, as the quality control standards of pharmaceutical ingredients allow to a less and less extent the presence of contaminations derived from intermediates, starting materials, side-products, optionally from isomers. As the intermediate for Ambroxol production is the 4-aminocyclohexanol *trans*-isomer, and owing to the above quality requirements, the formation of *cis*-isomers and by-products is not desired, their complete removal being a very significant task. So, the practical way of synthesizing Ambroxol would be to use a starting material free of *cis*-isomer

* Corresponding author. Tel.: +34 91 585 4765; fax: +34 91 585 4760.
*E-mail address:* irodriguez@icp.csic.es (I. Rodríguez-Ramos).

0920-5861/$ – see front matter © 2004 Elsevier B.V. All rights reserved.
doi:10.1016/j.cattod.2004.06.046

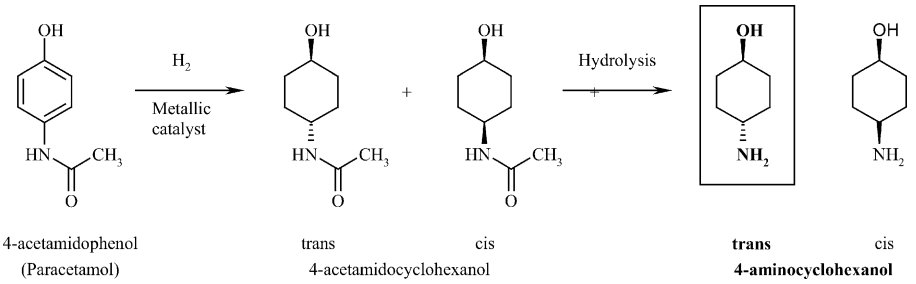


Fig. 1. Synthesis of *trans*-4-aminocyclohexanol by catalytic hydrogenation of 4-acetamidophenol (Paracetamol).

at the earliest step of the multistage synthesis, as the purification of the intermediates of the following synthesis steps requires much more work and time and results in higher yield and economic losses.

The stereoselectivity on the hydrogenation reaction of Paracetamol, as far as the *cis* and *trans* isomers ratio is concerned, depends on the metal catalyst, the type of support, and the employed reaction conditions. The information about catalysts compositions and conditions employed for this reaction is very scarce, and mainly patents are found in which no specifications are available, as far as basic research is concerned. The catalysts that appear in the patent literature, for the synthesis of *trans*-4-acetamidocyclohexanol and *trans*-4-aminocyclohexanol, are based on non-noble metals such as Ni and/or Co [11,12], Raney-Ni [13–15], and noble metals such as Pd on charcoal [9], Pt oxide [13], and Rh on $Al_2O_3$ [13].

In our attempt to design a more selective and/or cheaper catalyst, and as our preliminary tests showed a higher activity for Ru based catalysts than for Pt and Pd, we have used as the noble active phase ruthenium. Ru based catalysts are used for the hydrogenation of substituted phenols [16,17] and anilines [18] to produce the corresponding alkylcyclohexanols and alkylcyclohexylamines, respectively. Also, the modification of the Ru active phase with Co and Ni has been carried out with the aim of improving the catalytic results.

It is well known that acidic oxide supports lead to strong metal–support interactions leading to metal segregation in bimetallic catalysts [19,20]. To avoid such effects, as well as secondary reactions associated with the surface acidity of supports, we have selected a high surface area graphite and a carbon molecular sieve as supports of Ru, Co and Ni monometallic catalysts, while graphite-supported Ru–Co and Ru–Ni bimetallic catalysts have been prepared and tested on the title hydrogenation reaction.

## 2. Experimental and methods

### 2.1. Catalysts preparation

Monometallic M*x*H and M*x*S (M = Ru, Co, Ni; $x$ = wt.% metal loading) and bimetallic samples Ru2M′*y*H (M′ = Co, Ni; $(2 + y)$ = wt.% total metal loading) were prepared by the incipient wetness technique by (co)impregnation of the carbon materials with metal salt/s water solutions ($Ru(NO)(NO_3)_3$, $Co(NO_3)_2{\cdot}6H_2O$, $Ni(NO_3)_2{\cdot}6H_2O$). A high surface area graphite, free of surface oxygen functional groups [21], here denoted as H (HSAG, $S_{BET} = 297\,m^2/g$; Lonza Ltd.) and a carbon molecular sieve, named here as S ($S_{BET} = 1500\,m^2/g$), were used as supports. This S carbon was synthesized by carbonisation of the copolymer Saran (90% vinylidene chloride-10% vinyl chloride; Aldrich) under inert conditions ($N_2$; $100\,cm^3$/min) at 1073 K, and further activated by 17 oxidation–decomposition cycles (oxidation under stream of air at 673 K and decomposition of surface oxygen groups in flowing $N_2$ at 1223 K) [22]. Characterisation of the oxygen surface functional groups of the Saran material was carried out by temperature-programmed desorption (TPD) following the gas evolution with a quadrupole mass spectrometer.

### 2.2. Catalysts characterisation

Temperature-programmed reduction (TPR) measurements were carried out in a quartz micro-reactor over 200–300 mg of prepared sample, under a continuous flow of $20\,cm^3$/min of a $H_2$/He gas mixture (10% $H_2$). The temperature was increased from room temperature up to 800 K at 2 K/min. $H_2$ consumption was measured by on-line gas chromatography (Varian 3400) using a thermal conductivity detector (TCD).

The catalysts mean particle size was determined by CO volumetric chemisorption. The CO chemisorption isotherms were determined volumetrically, using an experimental system described elsewhere [23], on the samples subjected to in situ reduction pretreatment in flowing $H_2$ at 673 and 773 K. Mean particle sizes where determined assuming spherical metal particles and M:CO = 1:1 stoichiometry.

### 2.3. Catalytic hydrogenation

Previous to the catalytic experiments, about 500 mg of the corresponding catalyst sample were activated under flowing hydrogen ($30\,cm^3$/min) at 673 (sample-400) or 773 K (sample-500) for 2 h in a fixed-bed micro-reactor. These two reduction temperatures were chosen in order to investigate the influence of the metal particle size on the catalytic per-

formance. The catalyst, so obtained, was manipulated carefully in order to avoid the oxidation of its surface. Then, it was autoclaved along with 500 mg of Paracetamol (4-acetamidophenol 98%; Research Chemical, Ltd.) and 130 ml of ethanol. The system was purged and pressured with He until the reaction temperature was reached. The catalytic reaction was performed at 393 K and 50 bar of $H_2$, keeping the total pressure at 50 bar by introducing $H_2$ gas during the reaction whenever necessary. Manual liquid samples were taken and analysed using a gas-chromatograph (Varian 3800) equipped with a flame ionisation detector (FID) and a capillary column.

## 3. Results and discussion

### 3.1. Samples characterisation

Characterisation of the Saran support by TPD-MS showed the presence of oxygen surface functional groups of the carboxylic acid, lactone, phenolic and carbonyl types [24–28] as shown in Fig. 2.

Figs. 3–5 show the TPR profiles of the carbon-supported Ru, Co and Ni monometallic samples.

Ru2S (Fig. 3) shows three main reduction peaks at ca. 360, 400 and 510 K, as well as a broad peak that starts at ca. 600 K. Since the first $H_2$ consumption peak (360 K) appears along with NO and $CO_2$, it can be assigned to the decomposition of the ruthenium precursor nitrates and of the supports surface oxygen functional groups (carboxylic acid and lactone types), respectively. The peak at 400 K would be due to reduction of Ru(III) to $Ru^0$ species and to decomposition of the supports surface oxygen functional groups (lactone type), as evolution of $CO_2$ is also observed. Detection of $CH_4$ besides consumption peak at 510 K and the broad band at high temperature, allows assignment of said peaks to gasification of supports surface carbon atoms around the metal particles, as previously reported for other carbon-supported ruthenium catalysts [21,29,30]. Also, detection of CO is observed (starting at ca. 690 K) due to decomposition of phenolic type surface groups of the Saran support.

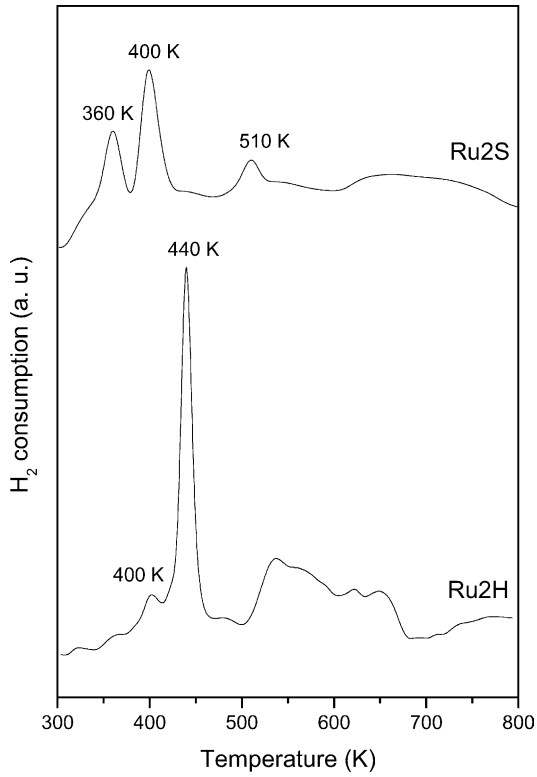


Fig. 3. TPR profiles of carbon-supported ruthenium monometallic samples.

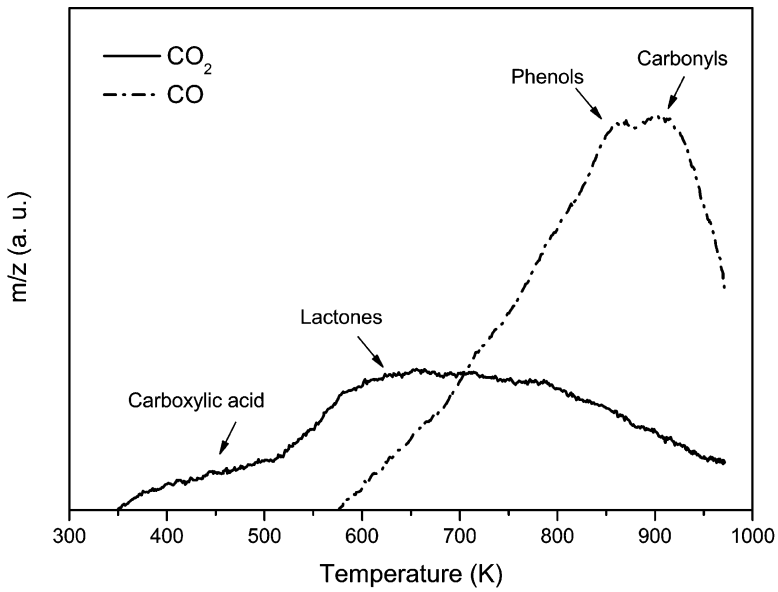


Fig. 2. TPD-MS profile of the Saran support: characterisation of surface functional groups.

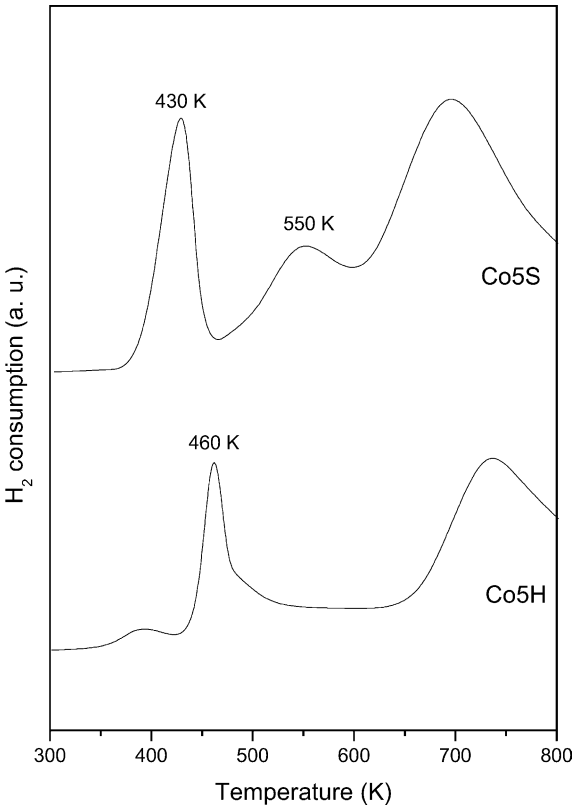


Fig. 4. TPR profiles of carbon-supported cobalt monometallic samples.

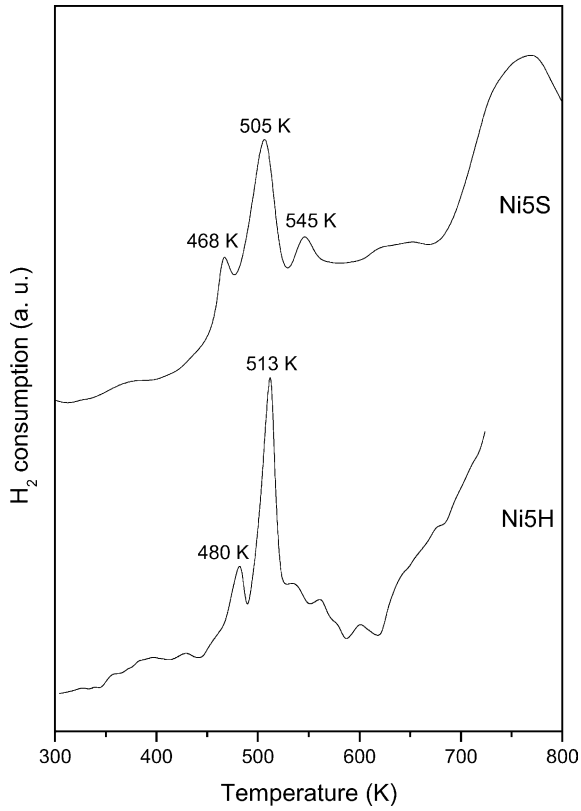


Fig. 5. TPR profiles of carbon-supported nickel monometallic samples.

Ru2H shows one main hydrogen consumption peak at ca. 440 K, with a small shoulder at ca. 400 K, and a broad peak for the 498–673 K range. The shoulder at 400 K will be due to decomposition of the precursor nitrates, since NO species are detected, while peak at 440 K is assigned to reduction of Ru(III) to $Ru^0$ species. Also, a small quantity of $CO_2$ is detected for the 400–440 K range due to the decomposition of surface groups of the support. These functional groups on the surface of the graphite support would have been generated by oxidation of surface carbon atoms by the NO species (generated by decomposition of the metal precursor). We have to take into mind that this support is clean of surface oxygen functional groups before the preparation of the samples [21]. On the other hand, the 498–673 K broad hydrogen consumption peak may be assigned to the gasification of carbon atoms of the graphitic support around the metal particles ($CH_4$ evolution).

The TPR profiles obtained for the carbon-supported Co samples (Fig. 4) do not show important differences. Peaks at ca. 430 and 460 K for Co5S and Co5H, respectively, are due to decomposition of the metal precursor (NO detection), reduction of Co(II) to $Co^0$ species, and decomposition of surface oxygen groups of the support ($CO_2$ evolution) of the carboxylic acid and lactone types. The broad peaks at ca. 600–900 and 630–900 K observed for Co5S and Co5H, respectively, as well as the 550 K peak for Co5S, may be ascribed to gasification of surface carbon atoms of the supports around the metal particles, since $CH_4$ production is detected. Also, production of CO was observed for Co5S starting at ca. 600 K, consequently due to the decomposition of phenolic type functional groups of the Saran support.

Similarly, carbon-supported Ni samples (Fig. 5) show peaks due to decomposition of precursor nitrates (ca. 468 and 480 K), reduction of Ni(II) to $Ni^0$ species (ca. 505 and 513 K) and decomposition of surface oxygen functional groups (almost from 300 up to ca. 560 K). The broad consumption peaks at high temperatures may be ascribed to gasification of carbon atoms of the supports in the vicinity of the metal particles (production of $CH_4$). For Ni5S, CO is also detected (ca. 650 K) due to decomposition of phenolic type surface groups of the support.

From these results we can conclude that the support has no influence on the reduction temperature of Co and Ni. The differences found for the Ru based samples may be due to specific interactions between the metal precursor and the Saran support.

Fig. 6 shows the TPR profiles of the bimetallic Ru–Co samples, compared to those of the corresponding counterparts. All Ru–Co samples show one main hydrogen consumption peak, suggesting that Ru and Co species are in intimate contact or else strongly interacting. But two trends may be observed depending on the cobalt loading. Samples with less cobalt content, Ru2Co0.5H and Ru2Co1H, are reduced at ca. the same temperature as Ru2H (440 K),

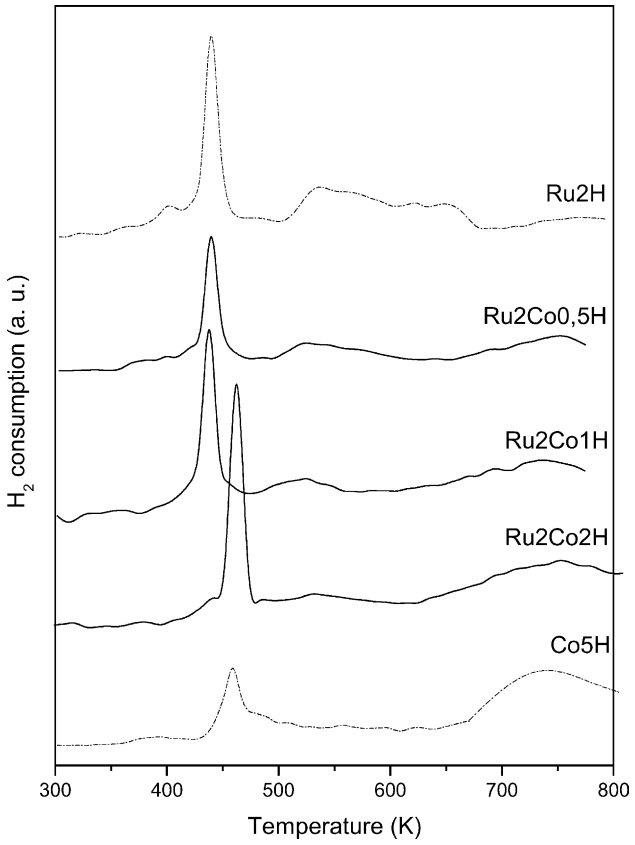


Fig. 6. TPR profiles of graphite-supported Ru–Co bimetallic samples (results of Ru2H and Co5H are also shown for comparison).

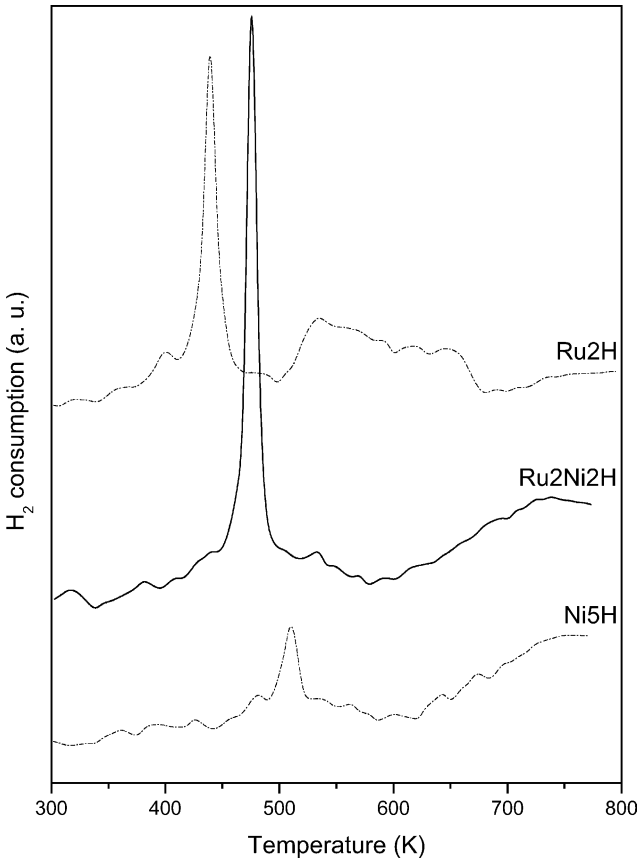


Fig. 7. TPR profile of the graphite-supported Ru–Ni bimetallic sample (results of Ru2H and Ni5H are also shown for comparison).

while Ru2Co2H is reduced at the same temperature as Co5H (460 K). For the former samples, it is quite clear that Co reducibility has been enhanced, what is in agreement with other studies carried out with silica [31,32] and alumina-supported [33] Ru–Co bimetallic samples. This phenomenon can be explained as follows: $Ru^0$ species, that are generated at low temperatures, are capable of chemisorbing hydrogen molecules and supply the H active species to Co(II) by a mechanism commonly known as "hydrogen spillover". Moreover, it has been proposed that the reduction of cobalt in the Ru–Co/$SiO_2$ sample by the hydrogen spillover effect can be due to formation of an alloy, that would make such spillover effect much easier [31,32]. For the latest (Ru2Co2H), the effect observed is the opposite, since cobalt delays the reduction of the ruthenium atoms. This suggests a Co enrichment as well as a strong interaction of Ru and Co atoms.

Bimetallic sample Ru2Ni2H (Fig. 7) shows one main consumption peak centred at ca. 480 K, that fits quite approximately with the mean temperature of the monometallic samples (440 and 513 K for Ru2H and Ni5H, respectively). These results are in good agreement with those found for silica-supported bimetallic Ru–Ni samples [34]. Again, the apparition of a sole reduction peak, convincingly shows that Ni and Ru must be strongly interacting or else very close together, suggesting the formation of bimetallic Ru–Ni particles. The formation of bimetallic Ru–Ni clusters has been suggested previously [35–37]. It can also be deduced that Ni reducibility has been enhanced by the spillover effect.

Table 1 shows the CO adsorption amount ($N_{ads}$; $\mu mol/g_{cat}$) and mean particle size ($d$; nm) determined by the CO chemisorption measurements for the carbon-supported monometallic samples reduced at 673 and 773 K. Sintering of metal particles is more pronounced for Co and Ni based samples compared to that of Ru. The carbon support seems to play no important role in dispersion, in agreement with the TPR results. Only Co5H, when reduced at 773 K, suffers a strong sintering of the metal particles, or else sto-

Table 1
CO adsorbed amount and mean particle size of carbon-supported Ru, Co and Ni monometallic samples, reduced at 673 and 773 K, as determined by CO chemisorption

| Sample | Reduced at 673 K | | Reduced at 773 K | |
|---|---|---|---|---|
| | $N_{ads}$ ($\mu mol/g_{cat}$) | $d$ (nm) | $N_{ads}$ ($\mu mol/g_{cat}$) | $d$ (nm) |
| Ru2S | 93 | 2.6 | 50 | 4.9 |
| Ru2H | 79 | 3.4 | 58 | 4.6 |
| Co5S | 125 | 6.4 | 44 | 18 |
| Co5H | 80 | 9.8 | 16 | 50 |
| Ni5S | 57 | 13 | 37 | 20 |
| Ni5H | 45 | 15 | 25 | 28 |

Table 2
CO adsorbed amount and mean particle size of graphite-supported Ru–Co and Ru–Ni bimetallic samples, reduced at 673 and 773 K, as determined by CO chemisorption

| Sample | Reduced at 673 K | | Reduced at 773 K | |
|---|---|---|---|---|
| | $N_{ads}$ (μmol/$g_{cat}$) | $d$ (nm) | $N_{ads}$ (μmol/$g_{cat}$) | $d$ (nm) |
| Ni5H | 45 | 15 | 25 | 28 |
| Ru2Ni2H | 65 | 9.4 | 24 | 25 |
| Ru2H | 79 | 3.4 | 58 | 4.6 |
| Ru2Co0.5H | 95 | 3.6 | 25 | 13 |
| Ru2Co1H | 100 | 4.3 | 37 | 12 |
| Ru2Co2H | 105 | 5.7 | 28 | 21 |
| Co5H | 80 | 9.8 | 16 | 50 |

ichiometry of CO adsorption changes. Results obtained for the graphite-supported bimetallic samples (Table 2) show how the addition of the second metal causes sintering of the metal particles, when compared to Ru2H, this strongly dependent on the amount of the second metal and reduction temperature. These results suggest that Co and Ni have a higher sintering capability than Ru. On the other hand, it is important to point out that the CO adsorption amount ($N_{ads}$) determined for the Ru–Co samples are very similar, independent of the Co loading.

### 3.2. Catalysts reactivity in the hydrogenation of Paracetamol

The catalytic hydrogenation of Paracetamol, under our experimental conditions, yields a mixture of *cis* and *trans*-4-acetamidocyclohexanol, *N*-cyclohexylacetamide and partial hydrogenation products (such as 4-acetamidocyclohexanone). According to the mechanism proposed by Tobicík and Cerveny [38] for the hydrogenation of alkyl-substituted phenols, and Neri et al. [39] for the hydrogenation of phenol, the hydrogenation of Paracetamol will follow the reaction scheme shown in Fig. 8.

Table 3 shows the catalytic results (intrinsic activity and selectivity values) in the hydrogenation of Paracetamol obtained with the monometallic catalysts when submitted to the studied reduction treatments. TOF values (specific activity) were calculated using CO $N_{ads}$ as the total surface metal sites. Selectivity values are divided in two parts:

(1) Chemoselectivity: for total hydrogenation ($S_H$), hydrogenolysis to *N*-cyclohexylacetamide ($S_N$) and partial hydrogenation ($S_{PH}$) reactions.
(2) Stereoselectivity in the total hydrogenation reaction ($S_T$ = (*trans*/(*cis* + *trans*)) × 100).

From the data shown in Table 3, it should be noted that, in general, the catalytic activity follows the trend Ru > Co ≫

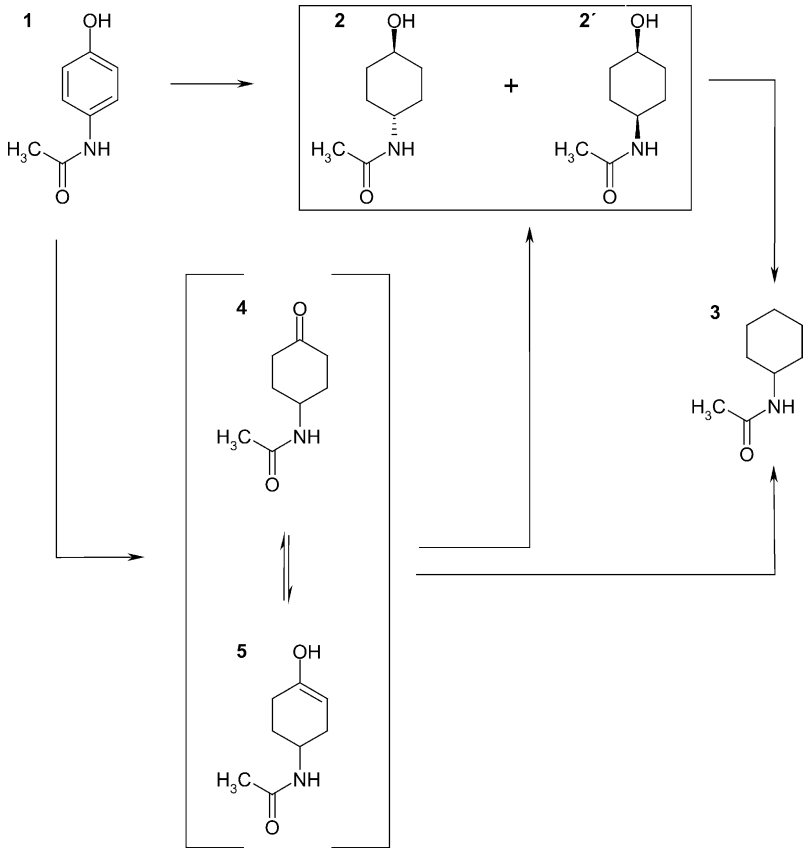


Fig. 8. Possible reactions in the hydrogenation of Paracetamol at 393 K (1: Paracetamol, 2: *trans*-4-acetamidocyclohexanol, 2′: *cis*-4-acetamidocyclohexanol, 3: *N*-cyclohexylacetamide, 4: 4-acetamidocyclohexanone, and 5: 4-acetamidocyclohexenol).

Table 3
Catalytic results of carbon-supported monometallic catalysts on the hydrogenation reaction of Paracetamol at 393 K

| Catalyst | $d$ (nm) | Intrinsic activity ($\mu$mol/$g_M$ s) | $TOF_{CO}$ ($s^{-1}$) | Chemoselectivity (%) | | | Stereoselectivity (%) | |
|---|---|---|---|---|---|---|---|---|
| | | | | $S_H$ | $S_N$ | $S_{PH}$ | $S_T$ | $S_C$ |
| Ru2S-400 | 2.6 | 93 | 0.020 | 55 | 39 | 6.0 | 42 | 58 |
| Ru2S-500 | 4.9 | 317 | 0.127 | 78 | 12 | 10 | 47 | 53 |
| Ru2H-400 | 3.4 | 21 | 0.005 | 87 | 9.0 | 4.0 | 49 | 51 |
| Ru2H-500 | 4.6 | 90 | 0.031 | 88 | 6.5 | 5.5 | 53 | 47 |
| Co5S-400 | 6.4 | 3.6 | 0.001 | 97 | 1.0 | 2.0 | 55 | 45 |
| Co5S-500 | 18 | n.d. | n.d. | 83 | 1.0 | 16 | 61 | 39 |
| Co5H-400 | 9.8 | 14 | 0.008 | 75 | 1.0 | 24 | 61 | 39 |
| Co5H-500 | 50 | 6.4 | 0.019 | 66 | 1.0 | 33 | 64 | 36 |
| Ni5S-400 | 13 | 1.4 | 0.001 | 88 | 3.0 | 9.0 | 51 | 49 |
| Ni5S-500 | 20 | n.d. | n.d. | 82 | 4.0 | 14 | 61 | 39 |
| Ni5H-400 | 15 | 2.0 | 0.002 | 91 | 2.0 | 7.0 | 59 | 41 |
| Ni5H-500 | 28 | n.d. | n.d. | 97 | 0.5 | 2.5 | 63 | 37 |

n.d.: non-determinable.

Ni, while chemoselectivity ($S_H$) follows the opposite trend. Generally, too, an increase in activity values is observed with particle size, particularly for Ru based catalysts, what seems to indicate that the reaction is structure sensitive.

All Ru catalysts are selective towards the total hydrogenation of the aromatic ring, but there are some important differences: Ru2S produces a very large amount of *N*-cyclohexylacetamide, particularly when it is reduced at 673 K (Ru2S-400). Since particle sizes of Ru catalysts, Ru2S-400 and Ru2H-400, are rather similar, these results may be only explained as due to the microporosity of the Saran support. Considering that the stereoisomers are rather big, the steric hindrance inside the pores will force further reaction to *N*-cyclohexylacetamide. The reduction treatment at 773 K causes sintering of metal particles and probably a migration towards the outer part of such pores. Steric hindrance decreases resulting in the production of a larger quantity of total hydrogenated products. Also, the presence of surface acidic functional groups (of the phenolic type), that have not yet decomposed with the reduction treatment at 673 K (see TPR results), could be responsible for *N*-cyclohexylacetamide production, by dehydration of the cyclohexanol derivative, as previously observed in the hydrogenation of phenol [39] with a $Pd/Al_2O_3$ catalyst.

Apart from the increase of $S_H$ with particle size, an increase in the *trans* composition is also observed for the Ru catalysts, mainly due to the decrease of the hydrogenolysis product ($S_{PH}$ increases only slightly), what fits well with the above discussion (the *trans* isomer is bigger than the *cis* form). These results suggest that hydrogenolytic cleavage is favoured over the small Ru particles and/or in the presence of acidic sites of the support. Also the adsorption mode of the Paracetamol molecule, that depends on the metal particle size (among other factors), has an effect on the selectivity values and will be explained later.

Results obtained with the Co based catalysts show that an increase in the metal particle size results in a decrease of $S_H$ and an increase in stereoselectivity towards the *trans* form. These results are in agreement with previously reported results on the hydrogenation of phenol [39,40] and on the competitive hydrogenation of toluene and benzene [41]. Shin and Keane [40] explain how the chemisorption mode of the phenol molecule (co-planar or non-planar to the catalysts surface) determines the selectivity of the reaction. In this way, a planar adsorption will favour formation of the cyclohexanol derivative, and to *cis* formation by hydrogen addition in one step [42]. On the other hand, a non-planar chemisorption mode (favoured over large metal particles) and hydrogen addition in various steps will lead to cyclohexanone and/or the *trans* stereoisomer formation [42]. Moreover, it has been proposed [39] that phenol hydrogenation takes place between phenol molecules chemisorbed on the support and hydrogen activated on the metal particles, and that depending on the Lewis acid–basic properties of the support, the adsorption mode is different: acidic properties lead to cyclohexanol formation (co-planar adsorption), while a basic character favours cyclohexanone formation by a non-planar adsorption.

Also, studies carried out by Richard et al. [41] on the competitive hydrogenation of toluene and benzene over different carbon-supported Pt based catalysts show that the ratio of the adsorption coefficients of toluene and benzene ($K_{T/B}$) depends on the electron density of the metal particles. In this sense, the lowest $K_{T/B}$ was obtained with a graphite-supported Pt catalyst. Since toluene is a better electron donor than benzene, the lower $K_{T/B}$ value is explained as due to a high electron density of the metal particles because of an electron transfer from the support, which is favoured when the metal particles are located at the edges of the graphite basal planes. Also a correlation with the selectivity results for the hydrogenation of cinnamaldehyde ($C_6H_5$–CH=CH–CHO) was carried out [41]. It was inferred that the higher selectivity towards cinnamyl alcohol ($C_6H_5$–CH=CH–$CH_2$OH) over the graphite-supported Pt catalysts was due to the high electron density of the metal aggregates, that lowers the probability of activation of the C=C

Table 4
Catalytic results of graphite-supported Ru–Co and Ru–Ni bimetallic catalysts on the hydrogenation reaction of Paracetamol at 393 K

| Catalyst | $d$ (nm) | Intrinsic activity ($\mu$mol/$g_M$ s) | $TOF_{CO}$ ($s^{-1}$) | Chemoselectivity (%) | | | Stereoselectivity (%) | |
|---|---|---|---|---|---|---|---|---|
| | | | | $S_H$ | $S_N$ | $S_{PH}$ | $S_T$ | $S_C$ |
| Ni5H-400 | 15 | 2.0 | 0.002 | 91 | 2.0 | 7.0 | 59 | 41 |
| Ni5H-500 | 28 | n.d. | n.d. | 97 | 0.5 | 2.5 | 63 | 37 |
| Ru2Ni2H-400 | 9.4 | 23 | 0.014 | 99.6 | 0.3 | 0.1 | 60 | 40 |
| Ru2Ni2H-500 | 25 | 10 | 0.017 | 99 | 0.5 | 0.5 | 65 | 35 |
| Ru2H-400 | 3.4 | 21 | 0.005 | 87 | 9.0 | 4.0 | 49 | 51 |
| Ru2H-500 | 4.6 | 90 | 0.031 | 88 | 6.5 | 5.5 | 53 | 47 |
| Ru2Co0.5H-400 | 3.6 | 53 | 0.014 | 88 | 4.0 | 8.0 | 52 | 48 |
| Ru2Co0.5H-500 | 13 | 40 | 0.039 | 83 | 6.0 | 11 | 53 | 47 |
| Ru2Co1H-400 | 4.3 | 37 | 0.012 | 89 | 4.0 | 7.0 | 53 | 47 |
| Ru2Co1H-500 | 12 | 33 | 0.026 | 86 | 5.0 | 9.0 | 55 | 45 |
| Ru2Co2H-400 | 5.7 | 42 | 0.016 | 90 | 4.0 | 6.0 | 53 | 47 |
| Ru2Co2H-500 | 21 | 7.2 | 0.010 | 84 | 5.0 | 11 | 56 | 44 |
| Co5H-400 | 9.8 | 14 | 0.008 | 75 | 1.0 | 24 | 61 | 39 |
| Co5H-500 | 50 | 6.4 | 0.019 | 66 | 1.0 | 33 | 64 | 36 |

n.d.: non-determinable.

bond. Also, steric effects due to the increase of the metal particle size may play a role on the adsorption modes of Paracetamol. The increase of the metal particle size increases the steric repulsion with the substituents of the aromatic ring, and so planar adsorption probability decreases [43].

Indeed, our Co catalysts show results that may be due to both effects, since there is a strong change in the mean particle sizes (and hence in the electron density), and the carbon supports have different acid–basic properties. The graphite material used in this study is an electron-donor support [44], while the Saran material contains acidic surface oxygen functional groups. The reduction treatment at 773 K of Co5S leads to sintering of metal particles and to the decomposition of such surface groups (see TPR results) losing the acidic character of Co5S-400. On the other hand, and taking in mind that the Saran support has no Lewis basic properties (even when no surface acidic functional groups are present) due to its irregular micrographitic structure, the similarity in particle sizes, chemoselectivity and stereoselectivity values of Co5S-500 and Co5H-400 suggests that the variations of the electron density (due to changes in the mean particle size) plays a more important role for the Co catalysts. The larger the metal particle, the higher the electron density (and higher the steric hindrance), and hence the probability of co-planar aromatic ring adsorption decreases.

Since the mean particle sizes found for the cobalt catalysts are in a range of sizes bigger than that found for Ru, the effects due to the adsorption mode over large metal particles and, consequently, the variations of $S_{PH}$ values observed for the Ru catalysts are less pronounced. Yet, results obtained with the Ru based catalysts agree with the above discussion. The increase in the particle size increases the electron density of the Ru particles and, consequently, $S_N$ decreases and $S_{PH}$ increases. The role of the supports Lewis acid–basic properties is important when metal particles are rather small, what is the case of Ru based catalysts. Note that for the Ru2S catalysts, selectivity is governed mainly by the microporosity and presence of acidic surface functional groups.

As for the Ni catalysts, a similar behaviour to that found for the Co catalysts is observed. Contrary to what was found for the hydrogenation of alkyl-substituted phenols with a $Ni/Al_2O_3$ catalyst [38], our Ni catalysts were poorly selective towards hydrogenolytic cleavage products because of their less acidic character.

All graphite-supported Ru–Co bimetallic catalysts show similar selectivity results independent of the Co loading and reduction temperature (Table 4). Chemoselectivity ($S_H$) and stereoselectivity values, in terms of the *trans* composition, are close to those of the Ru2H catalysts, the effect of the mean particle sizes not being observed. These results suggest that the catalytic reaction is governed by ruthenium metal particles, or else (and as the CO adsorbed amounts determined for these bimetallic catalysts suggest) by bimetallic Ru–Co clusters or Ru–Co alloyed particles.

Graphite-supported Ru–Ni bimetallic catalysts are much more selective ($S_H$ and $S_T$) than the Ru2H and Ni5H catalysts, leading almost completely to the total hydrogenation products. For this bimetallic system too, the increase in the metal particle size leads to an enhancement of the *trans* fraction. It is worth noting that, among the catalysts used in this study, Ru2Ni2H-500 gives the highest T/C ratio.

## 4. Conclusions

In this paper we show that the parameters affecting the hydrogenation of 4-acetamidophenol to yield the desired stereoisomer of 4-acetamidocyclohexanol can be controlled by selecting the proper bimetallic system. Also, the support material, the reduction temperature treatment and the result-

ing metal particle sizes (as determined by CO chemisorption) may contribute to maximize the desired catalytic properties, particularly the stereoselectivity.

## Acknowledgements

MCA would like to thank the Universidad Nacional de Educación a Distancia (UNED) in Spain for a scholarship grant (Convocatoria 1999). The financial support of the MC&T of Spain under project MAT 2002-04189-C02-01 and 02 is recognized.

## References

[1] T. Weiser, N. Wilson, Mol. Pharmacol. 62 (2002) 433.
[2] B. Yang, D.F. Yao, M. Ohuchi, M. Ide, M. Yano, Y. Okumura, H. Kido, Eur. Resp. J.: Off. J. Eur. Soc. Clin. Resp. Physiol. 19 (2002) 952.
[3] H. Narahara, M. Tatsuta, H. Iishi, M. Baba, T. Mikuni, N. Uedo, N. Sakai, H. Yano, Cancer Lett. 168 (2001) 117.
[4] A. Moroni, Magis Farmaceutici S.R.L., Brescia, Italy, US Patent 4 528 393 (1985).
[5] J. Rocas-Sorolla, I. Valls-Sanahuja, E. Fernández-Guerra, Servicios y Suministros Farmacéuticos S.A., Barcelona, Spain, Span. ES 2 002 438 (1988).
[6] J. Kech, Liebigs Ann. Chem. 707 (1967) 107.
[7] Servicios y Suministros Farmacéuticos S. A., Barcelona, Spain, ES 549 316 (1986).
[8] J. Prats-Palacin, J.M. Valles-Plana, Laboratorios Lasa S. A., Spain, ES 544 291 (1986).
[9] I. Ratz, P. Benko, D. Bozsing, A. Tungler, T. Mathe, G. Kovanyi, J. Petro, I. Sztruhar, G. Vereczkey, EGIS Gyogyszergyar, Hungary, Brit. UK Patent Appl. GB 2 239 242 (1991).
[10] I. Ratz, P. Benko, D. Bozsing, A. Tungler, T. Mathe, G. Kovanyi, J. Petro, I. Sztruhar, G. Vereczkey, EGIS Gyogyszergyar, Hungary, Brit. UK Pat. Appl. GB 2 239 241 (1991).
[11] Firm Soc. Chemical Industry, Basel, Switzerland, Eur. Pat. Specif. GB 454 042 (1936).
[12] H. Ensslinn, M. Hartmann, L. Panizzon, Firm Soc. Chemical Industry, Basel, Switzerland, US 2 152 960 (1939).
[13] B. Lehmann, Great Lakes Chemical Konstanz G. m. b. H., Denmark, EP 0 909 753 (1999).
[14] R.R. Fraser, R.B. Swingle, Can. J. Chem. 48 (1970) 2065.
[15] J. Yang, Jingxi Huagong 17 (2000) 100.
[16] B. Breitscheidel, T. Rühl, K. Flick, J. Henkelmann, A. Henne, R. Lebkücher, BASF Aktiengesellschaft, Denmark, US 5 874 622 (1999).
[17] H. Rütter, T. Rühl, B. Breitscheidel, J. Henkelmann, T. Wettling, BASF Aktiengesellschaft, Ludwigshafen, Denmark, US 5 942 645 (1999).
[18] G.M. Whitman, E. I. Du Pont de Nemours & Company, Wilmington, Delaware, US 2 606 925 (1952).
[19] J. Phillips, J. Weigle, M. Herskowitz, S. Kogan, Appl. Catal A Gen. 173 (1998) 273.
[20] S.M. da Silva, J. Phillips, J. Mol. Catal. 94 (1994) 97.
[21] A. Guerrero-Ruíz, P. Badenes, I. Rodríguez-Ramos, Appl. Catal. A Gen. 173 (1998) 313.
[22] I. Fernández-Morales, A. Guerrero-Ruíz, F.J. López-Garzón, I. Rodríguez-Ramos, C. Moreno-Castilla, Appl. Catal. 14 (1985) 159.
[23] B. Bachiller-Baeza, I. Rodríguez-Ramos, A. Guerrero-Ruíz, Langmuir 14 (1998) 3556.
[24] J.L. Figueiredo, M. Pereira, M. Freitas, J. Orfao, Carbon 37 (1999) 1379.
[25] G.S. Szymanski, Z. Karpinski, S. Biniak, A. Swiatkowski, Carbon 40 (2002) 2627.
[26] J.L. Lemaitre, in: F. Delanay, et al. (Eds.), Characterisation of Heterogeneous Catalysts, vol. 28, Marcel Dekker, New York, 1984.
[27] A. Aksoylu, M. Madalena, A. Freitas, M. Pereira, J.L. Figueiredo, Carbon 39 (2001) 175.
[28] U. Zielke, K.J. Huttinger, W. Hoffman, Carbon 34 (1996) 983.
[29] B. Bachiller-Baeza, A. Guerrero-Ruíz, P. Wang, I. Rodríguez-Ramos, J. Catal. 204 (2001) 450.
[30] B. Bachiller-Baeza, I. Rodríguez-Ramos, A. Guerrero-Ruíz, Appl. Catal. A Gen. 205 (2001) 227.
[31] N. Tsubaki, S. Sun, K. Fujimoto, J. Catal. 199 (2001) 236.
[32] X. Qiu, N. Tsubaki, S. Sun, K. Fujimoto, Fuel 81 (2002) 1625.
[33] L. Guczi, R. Sundararajan, Zs. Koppány, Z. Zsoldos, Z. Schay, F. Mizukami, S. Niwa, J. Catal. 167 (1997) 482.
[34] C. Crisafulli, S. Scirè, S. Minicò, L. Solarino, Appl. Catal. A Gen. 225 (2002) 1.
[35] C. Crisafulli, S. Scirè, R. Maggiore, S. Minicò, S. Galvagno, Catal. Lett. 59 (1999) 21.
[36] D.J. Elliot, J.H. Lunsford, J. Catal. 57 (1979) 11.
[37] J.M. Rynkowski, T. Paryjczak, M. Lenik, Appl. Catal. 126 (1995) 257.
[38] J. Tobicík, L. Cerveny, J. Mol. Catal. A Chem. 194 (2003) 249.
[39] G. Neri, A.M. Visco, A. Donato, C. Milone, M. Malentacchi, G. Gubitosa, Appl. Catal. A Gen. 110 (1994) 49.
[40] E.-J. Shin, M.A. Keane, J. Catal. 173 (1998) 450.
[41] D. Richard, P. Gallezot, D. Neibecker, I. Tkatchenko, Catal. Today 6 (1989) 171.
[42] T.J. Donohoe, R. Garg, C.A. Stevenson, Tetrahedron: Asymmetry 7 (1996) 317.
[43] C. Minot, P. Gallezot, J. Catal. 123 (1990) 341.
[44] A. Guerrero-Ruíz, A. Maroto-Valiente, M. Cerro-Alarcón, B. Bachiller-Baeza, I. Rodríguez-Ramos, Top. Catal. 19 (2002) 303.